ACS APPLIED MATERIALS & INTERFACES

Research Article

www.acsami.org

Investigation of Fluoroethylene Carbonate Effects on Tin-based Lithium-Ion Battery Electrodes

Zhenzhen Yang,[†] Andrew A. Gewirth,[‡] and Lynn Trahey*[,†]

[†]Chemical Science and Engineering Division, Argonne National Laboratory, 9700 South Cass Avenue, Lemont, Illinois 60439, United States

[‡]Department of Chemistry, University of Illinois, 600 South Mathews Avenue, Urbana, Illinois 61801, United States

ABSTRACT: Electroless plating of tin on copper foil (2-D) and foams (3-D) was used to create carbon- and binder-free thin films for solid electrolyte interphase (SEI) property investigation. When electrochemically cycled vs lithium metal in coin cells, the foam electrodes exhibited better cycling performance than the planar electrodes due to electrode curvature. The effect of the additive/cosolvent fluoroethylene carbonate (FEC) was found to drastically improve the capacity retention and Coulombic efficiency of the cells. The additive amount of 2% FEC is enough to derive the benefits in the cells at a slow (C/9) cycling rate. The interfacial properties of Sn thin film electrodes in electrolyte with/without FEC additive were investigated using in situ electrochemical quartz crystal microbalance with dissipation (EQCM-D). The processes of the decomposition of the electrolyte on the electrode surface and Li alloying/dealloying with Sn were characterized quantitatively by surface mass change at the molecular level. FEC-containing electrolytes deposited less than electrolyte without FEC on the initial reduction sweep, yet increased the overall thickness/mass of SEI after several cyclic voltammetry cycles. EQCM-D studies demonstrate that the mass accumulated per mole of electrons (mpe) was varied in different voltage ranges, which reveals that the reduction products of the electrolyte with/without FEC are different.

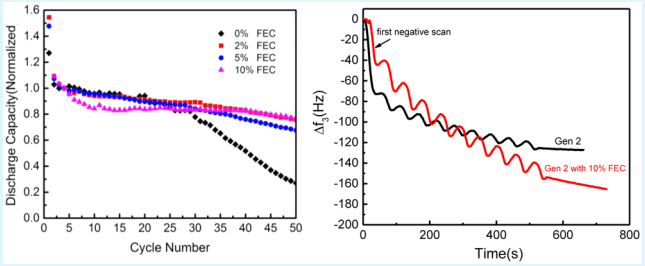

KEYWORDS: *FEC additive, tin anode, electrochemical quartz crystal microbalance, EQCM-D, LIB*

1. INTRODUCTION

Graphite has been commonly used as the anode material in commercial Li-ion rechargeable batteries for many years.[1] Nevertheless, graphite cannot fulfill requirements for higher storage capacity owing to its intrinsic limitation in lithiation capacity.[2] Naturally, many groups are interested in developing alternative anodes that can provide enhanced performance while still possessing the desired stability and safety characteristics. Among various anode materials, silicon and tin are widely researched, high specific capacity replacements to carbonaceous anodes in Li-ion batteries.[3−5] However, direct employment of Si or Sn in Li-ion batteries is hindered by their limited cycle life, which is due to material degradation brought on by severe volume changes during repeated lithiation and delithiation.[6] Ideas for ways to minimize the deleterious effects of the volume change include using a second inactive phase to buffer the expansion and engineering three-dimensional electrode architectures with sufficient porosity to accommodate the excessive volume changes occurring during the charge−discharge cycles.[6−13] In this study, copper current collectors with a 3-D foam structure conformally coated with very thin films of active material were used to enhance the electrochemical performance of Sn electrodes. Although not suitable for replacing state of the art graphite anodes, our electrodes are carbon- and binder-free, and thus are engineered to enable insight into the phenomenon of solid electrolyte interphase (SEI) formation.

Electrolyte additives are one of the most promising and effective ways for improving the performance of Li-ion batteries.[14] For example, research has shown that discharge capacity retention and Coulombic efficiency are remarkably improved by the addition of fluoroethylene carbonate (FEC) and vinylene carbonate (VC) for Si-based and carbon-based cells.[15−20] Various techniques have been established to study additive effects on the SEI, such as Fourier transform infrared (FTIR), X-ray photoelectron spectroscopy (XPS), atomic force microscopy (AFM), spectroscopic ellispsometry, and mass spectrometry.[15,16,21−23] Although the beneficial role of anode SEI additives has been demonstrated, the exact mechanisms underlying the improvements are not understood beyond some broad areas of agreement.[24] For instance, SEI formation on silicon electrodes cycled with the FEC additive have been studied with both XPS and spectroscopic ellipsometry (SE) with contradictory conclusions. Many discrepancies focus on whether FEC increases the SEI thickness and LiF composition on Si anodes.[24] Nakai et al. found that electrolytes containing FEC form very thin SEI layers compared to those formed by ethylene carbonate electrolytes.[15] In contrast, the SEI layer is

Received: December 5, 2014
Accepted: March 5, 2015
Published: March 5, 2015

DOI: 10.1021/am508593s
ACS Appl. Mater. Interfaces 2015, 7, 6557−6566

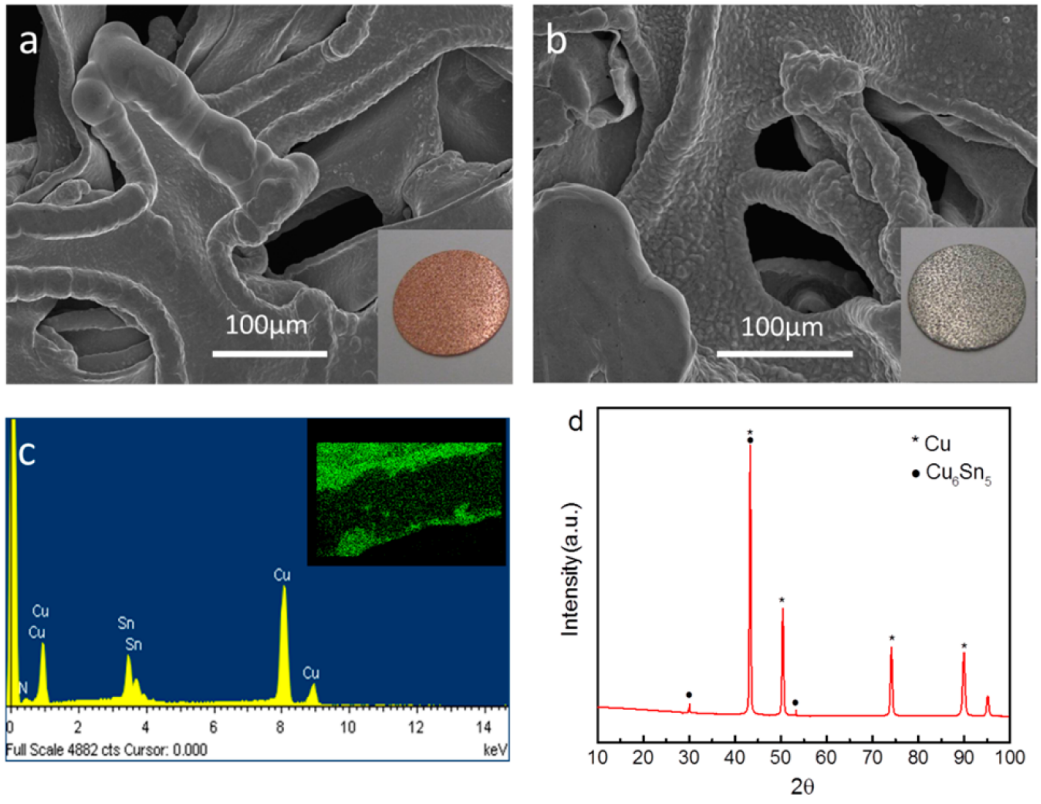

Figure 1. (a) SEM image of the uncoated 3D porous Cu foam. (b) SEM image of the Cu foam after coating with a thin layer of Sn. (c) EDS spectrum of coated foam cross section. (d) XRD pattern of the synthesized Sn thin layer on porous Cu foam.

thicker on anodes cycled in electrolyte with FEC revealed by the SE technique.[16]

Although surface-sensitive methods are valuable, it is often difficult to quantify mass gain/loss and the timing of those changes as they relate to applied current or voltage. One of the more direct ways of probing the chemical and electrochemical reactions is to use electrochemical quartz crystal microbalance (EQCM). In EQCM lies the possibility of detecting the in situ surface mass change of an electrode involved in an electrochemical process.[25,26] In this work, we employ electrochemical quartz crystal microbalance coupled with dissipation monitoring (EQCM-D). In addition to the frequency, EQCM-D uniquely measures a second parameter, dissipation (D) on the electrode, which is related to the properties of interfacial films such as rigidity and viscoelasticity. By including a set of frequency overtones in the measurement, we effectively probe different depths of the deposited layer which allows for a more detailed analysis of the SEI properties. Herein we use EQCM-D to compare the SEI formation on tin electrodes as a function of FEC concentration in the electrolyte. These first studies utilizing in situ EQCM-D for Li-ion battery anode materials will ultimately be a useful addition to the library of SEI characterization information.

2. EXPERIMENTAL SECTION

Sn-based electrodes were prepared by electroless tin plating on Cu foam/foil for 60 s from the Caswell plating bath at 50 °C. The surface of the Cu was cleaned by soaking in a dilute HCl solution followed by acetone before Sn coating. The deposition rate is determined by bath temperature, which was held steady for each batch. Large area foil and foams were coated in a batch process before punching electrodes, each batch producing 12+ electrodes. The Sn electrodes were washed thoroughly with water and acetone and then dried with air flow. Sn electrodes were stored overnight in a vacuum oven at 70 °C. The electrochemistry of the material was studied using 2032 coin cells. The electrodes were punched into 1.4 cm diameter discs. Lithium foil was used as the negative/counter electrode. The positive and negative electrodes were separated by two layers of separator (Celgard 2325). Cells were cycled in "Gen 2" electrolyte with and without additives at room temperature. The Gen 2 electrolyte (1.2 M $LiPF_6$ in a mixture of ethylene carbonate (EC) and ethyl methyl carbonate (EMC) (3:7 by weight)) was used as received without further purification (Tomiyama High Purity Chemical Industries Ltd.). Fluoroethylene carbonate (FEC, Alfa Aesar, 98%) containing electrolytes were prepared by adding different amounts FEC: 2 wt %, 5 wt %, 10 wt % into Gen 2 in a dry argon atmosphere glovebox. Once assembled, the cells rested for 1 h to enable complete wetting of the electrochemically active surfaces, and then cycled from open circuit potential (OCP) to 10 mV (lithiation). Extended cycling was conducted for 50 cycles between 10 mV and 1.5 V vs lithium metal at different current densities (0.03, 0.06, and 0.27 mA/cm^2) using a MACCOR 4000 battery cycler.

EQCM-D measurements were carried out with a two-electrode electrochemical cell (E1 module, Q-sense). Cu-coated, planar AT-cut quartz crystals with a basic resonant frequency 5.0 MHz were coated with electroless tin and used as the working sensor (Biolin Scientific). The same electroless method described above was used to deposit a thin layer of Sn (4 s plating) on Cu quartz crystals for EQCM. The Sn thin film electrodes were washed thoroughly with water and acetone and then dried with air flow. A thin layer of Li was deposited onto the Pt electrode from Gen 2 electrolyte at a constant current 0.001 A for 10 min, which was used as the counter electrode. The seal between the crystal and the Li/Pt counter in the cell was achieved with Kalrez O-rings (Biolin Scientific), leaving an exposed geometric area of 1.13 cm^2 of the Sn−Cu film in contact with the electrolyte. Kalrez O-rings were found to be resistant to swelling in the presence of the organic electrolytes used here. The commercial QCM-D apparatus allows simultaneous measurements of changes in the resonance frequency (Δf) and in the energy dissipation (ΔD). The quartz crystal can be excited to oscillate in thickness-shear mode at its fundamental

DOI: 10.1021/am508593s
ACS Appl. Mater. Interfaces 2015, 7, 6557−6566

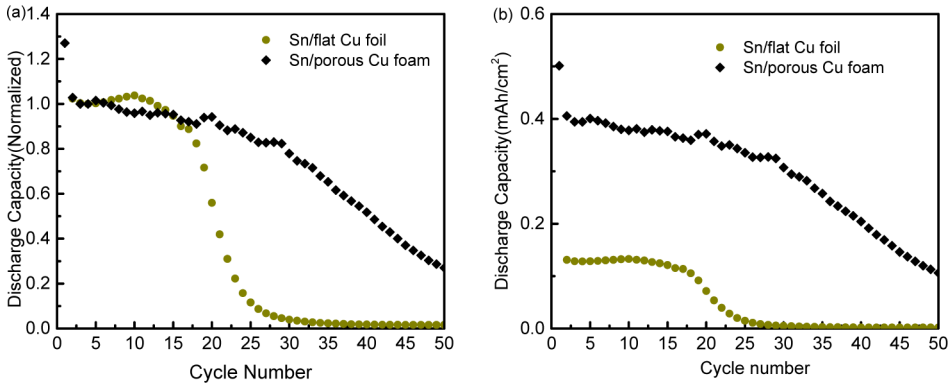

Figure 2. Normalized discharge capacity in (a) and capacity in mAh/cm^2 (areal) in (b) vs cycle number of the Sn/porous Cu electrode (3-D) and that of Sn/flat Cu electrode (2-D) at a current density of 0.03 mA/cm^2, voltage range between 0.01 and 1.5 V vs Li.

resonance frequency (f_1 = 5 MHz) and odd overtones (n = 3, 5, 7, 9, 11, 13) by applying an rf voltage across the electrode. All overtones show the same tendency of frequency shifts during the measurements, which indicate that the processes governing the responses occur homogeneously over the Sn−Cu surface. The resonant frequency of the EQCM sensor was measured with an accuracy of 0.1 Hz, which corresponds to a mass change sensitivity of 1.8 ng/cm^2.

To elucidate the effect of the additive, measurements were carried out in Gen 2 electrolyte with and without 10 wt % FEC at 25 °C. Prior to cyclic voltammetry, the electrolyte was injected into the EQCM chamber and allowed to rest until the QCM frequency stabilized. A CH potentiostat (Model 660) was used to control the electrical potential. The CV used a scan rate of 100 mV/s for 10 cycles between the OCP (~3 V vs Li^+/Li^0) and 100 mV. All measurements were carried out in a glovebox with dry argon atmosphere.

3. RESULTS AND DISCUSSION

3.1. Characterization of Sn Electrode and Basic Electrochemical Performance. Thin layers of tin were coated onto ~100 μm-thick macroporous Cu foams via electroless deposition. Figure 1a shows the scanning electron microscopy (SEM) image of the uncoated Cu substrate, displaying a three-dimensional interconnected macroporous structure with internal spacings of 100−200 μm. The inset shows a photograph of the Cu foam disc. The Cu substrates were immersed in the Caswell plating bath for 60 s, turning the copper foam silver in color, as shown in the inset of Figure 1b. Compared with electrodeposition, electroless plating is relatively simple immersion method to conformally deposit Sn onto Cu.[27] Figure 1b shows that the Sn coating mimics the Cu substrate, indicating the coating is conformal and thin. EDS mapping for a cross section of the coated foam is shown in Figure 1c. The Sn and Cu distribution is different in the overlapped mapping image, in which a thin layer of Sn (green) uniformly covers on the surface of Cu film (blue/black). The thickness of the Sn film is about 2 μm. Figure 1d shows the corresponding X-ray diffraction (XRD) pattern of the as-deposited Sn electrode on Cu foam. XRD data does not show individual Sn peaks, but Cu_6Sn_5 character was detected at 30° and 43° (JCPDS No. 45-1488).[27] It is likely that the Cu_6Sn_5 intermetallic compound, which is a stable binary phase at room temperature, formed between tin and copper during the electroless-plating process. It is also expected and confirmed by the voltammetry that the remaining amorphous Sn is oxidized due to the nature of the plating and the air exposure. Tin oxides undergo conversion reactions (the oxygen lithiates to form Li_2O) followed by the Sn−Li alloying reaction.[28−30] For simplicity, the complex $Cu/Cu_6Sn_5/SnO_x$ electrodes will be referred to as Sn, although it is important to note that the oxide surface, which is the same for all experiments reported herein, is the true surface for the initial measurements. Using the 3-D porous current collector we expect this thin layer of active Sn has better elasticity to effectively accommodate the strain of volume change during Li^+ insertion/extraction.

Figure 2 displays the electrochemical performance of the 3-D porous Sn/Cu electrode. For comparison, the cycle performance of the Sn electrode deposited on a flat and smooth Cu foil (2-D) is also shown. The capacities are normalized at the fourth cycle to justify for cell-to-cell variations resulting from differences in electrode loading, allowing the rate of fade to be prominent. The total areal capacity (Figure 2b) of the foam is higher than that of the foil due to the increased copper surface area, yet the thickness of tin on the two different substrates is relatively the same as it is based on electroless bath deposition rates, barring diffusion limitations in the foam interior. Similar to other reports, the reversible capacity for the Sn electrode deposited onto smooth Cu foil is abruptly degraded after 16 cycles due to large Li-driven volume variations during the lithiation/delithiation processes.[6] This problem has been a major challenge for Sn-based anodes in Li-ion batteries. The 3-D macroporous Sn/Cu electrode shows enhanced capacity retention relative to the 2D film in the first 30 cycles. The results confirm that compared to the flat Cu foil, curved Cu is a more suitable as a current collector for Sn anode because the material expansion is not entirely limited to one direction normal to the Cu.[6,7]

3.2. Effect of FEC Additive on Electrochemical Performance. Although the Sn/porous Cu composite electrode delivered a stable capacity during the early cycles, there was an abrupt onset of capacity fade at cycle 30. The loss of electrochemical capacity after 30 cycles is partially related to the degradation of the lithium metal counter electrode, which suffers from impedance rise due to extensive SEI formation at this electrode during repeated plating.[6] Additionally, there is also the possibility that electronic contact is lost between some of the Sn/Cu particles and the Cu foam substrate during prolonged electrochemical cycling due to the formation of a particle encapsulating, electrically resistive SEI layer.[31]

Recent research shows fluoroethylene carbonate (FEC) can significantly improve the cycle life and enhance the thermal stability of Si-based electrodes by facilitating SEI formation.[17,19,32−34] To investigate the effect of electrolyte additives on the cell performance, half cells (3-D Sn/Cu vs Li) with different amounts of FEC in the battery electrolyte were

DOI: 10.1021/am508593s
ACS Appl. Mater. Interfaces 2015, 7, 6557−6566

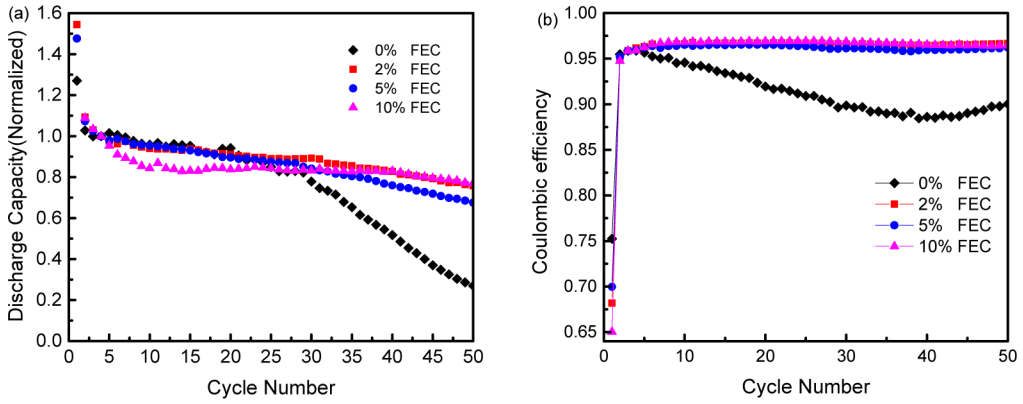

Figure 3. Plots of (a) discharge capacity and (b) Coulombic efficiency vs cycle number with 2%, 5%, 10% FEC addition (weight %) in the electrolytes, all cycled at 0.03 mA/cm^2. Retention of the discharge capacity of the cell can be enhanced by the introduction of FEC additive to the electrolyte solution and the overall Coulombic efficiency is also improved. Discharge capacities normalized on the 4th cycle.

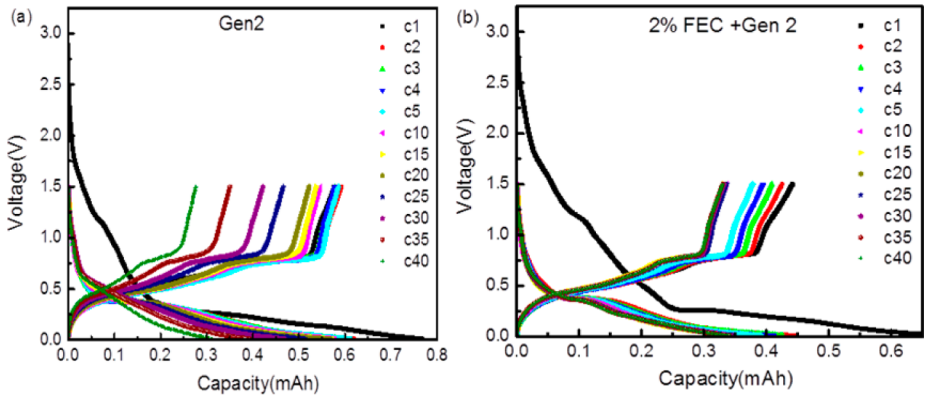

Figure 4. Voltage profiles of Sn/Cu foam cycled at 0.03 mA/cm^2 between 0.01 and 1.5 V vs Li in (a) Gen 2 and (b) 2% FEC in Gen 2, during 1st–5th cycles, 10th, 15th, 20th, 25th, 30th, 35th, and 40th cycles.

galvanostatically cycled between 0.01 and 1.5 V at 0.03 mA/cm^2 (C/15), as shown in Figure 3. The discharge capacity was normalized on the fourth cycle, as shown in Figure 3a. Without FEC, the cell retains its >80% capacity in first 30 cycles. However, the discharge capacity of the half cells without FEC dramatically decays after 30 cycles. The cell steadily loses its capacity at a rate of 0.5% per cycle. The cells containing FEC show similar capacity retention in the first 30 cycles, demonstrating that the addition of FEC does not change the initial discharge–charge cycling characteristics in any significant manner. However, a distinct trend can be seen after 30 cycles: capacity retention is clearly improved when FEC is present in long-term cycling. Among the cells with three different FEC concentrations, the 2 wt % addition shows the best overall performance (highest average and final discharge capacity) over 50 cycles.

Long-term Coulombic efficiencies are also improved when FEC is added to the electrolyte, as shown in Figure 3b. The Coulombic efficiency is a measure of how much lithium is trapped at the electrode after delithiation, either from incorporation into the SEI or electronic isolation of lithiated tin particles. During the first two cycles, when the original SEI is formed, the Coulombic efficiencies without FEC are slightly higher than those of cells with FEC. From Figure 3b, we can see that the Coulombic efficiency of FEC-free cells decreases steadily after initial SEI formation, reaching 89% after 50 cycles. By contrast, the cells containing FEC retains 95% efficiency over 50 cycles. The cells with 2%, 5%, and 10% FEC are virtually the same after 50 cycles, indicating that varying the concentration effect of FEC from 2 to 10 wt % does not impact Coulombic efficiency between the cells of the same negative electrode, but does increase discharge capacity retention. Because choosing the optimal amount of electrolyte additive is a balancing act between Coulombic efficiency and discharge capacity, it was concluded that the half cells with 2% FEC exhibit the best overall performance for this porous Sn-based anode at a slow discharge–charge rate (C/15) from both of results.

Overall, the electrochemical measurements on the porous Sn electrode described in this work indicate that presence of FEC in the solutions plays beneficial roles in decreasing the irreversible capacity of these electrodes while improving of the reversibility of Li^+ insertion/extraction. There are two metals in the half cell, however; lithium metal is also benefiting from the FEC addition in terms of capacity retention and Coulombic efficiency. The effect of the FEC on the tin electrode will be isolated with the help of the EQCM-D, in section 3.4.

Figure 4 details representative voltage profiles at a relatively slow cycling rate (C/15) for the cells free of FEC (Figure 4a) and with 2% FEC (Figure 4b). The initial discharge/charge curves for both cells are very similar. However, steadier cycling (less span in voltage ranges) over time can be obtained with FEC, which suggests additives affect the anode electrochemistry on long-term cycling rather than only on the first cycle.[35] In the course of the first discharge process, the cell potential

DOI: 10.1021/am508593s
ACS Appl. Mater. Interfaces 2015, 7, 6557–6566

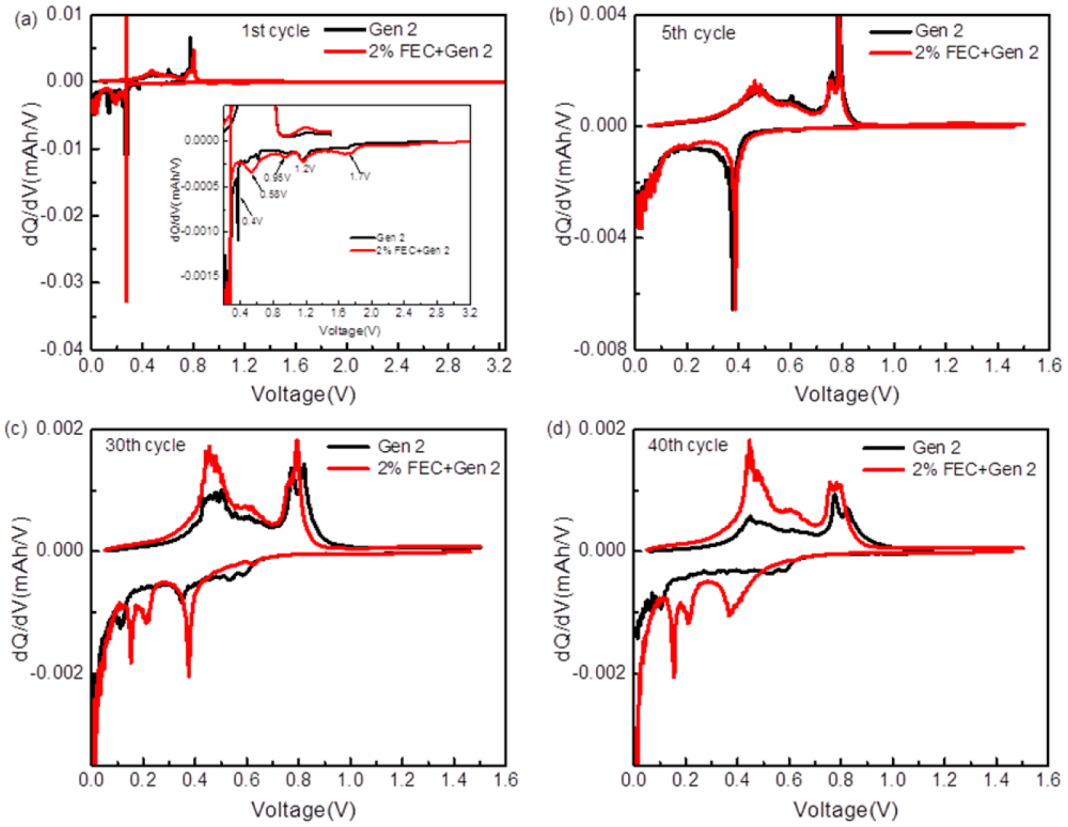

Figure 5. Comparison of differential capacity plots (dQ/d*V*) of half cells with 0 and 2%, FEC: (a) initial cycle, (b) 5th cycle, (c) 30th cycle, and (d) 40th cycle.

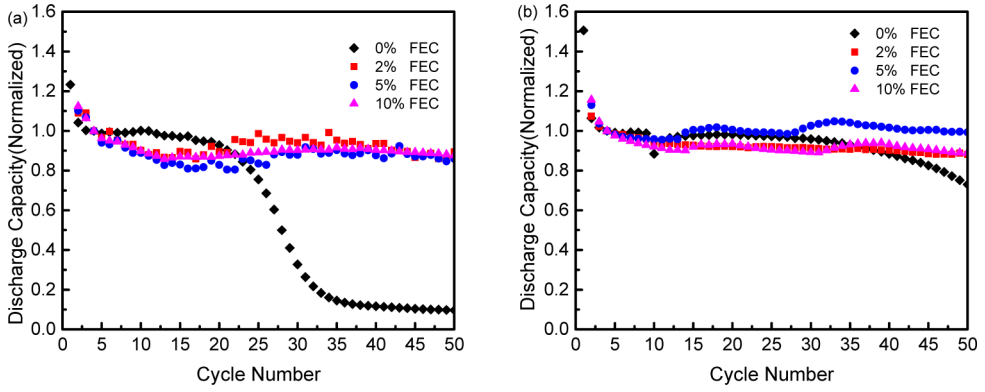

Figure 6. Normalized discharge capacity vs cycle number of the Sn/porous Cu with 2%, 5%, and 10% FEC at different cycling rates: (a) 0.06 mA/cm^2 (C/9) and (b) 0.27 mA/cm^2 (C/2).

immediately drops from OCP to 2.0 V after starting the test, and then gradually falls toward 0.01 V for both of the cells. An obvious potential plateau at 1.2 V can be observed for the cell with or without additive present, which is assigned to the decomposition of ethylene carbonate.[36] This point is clearly shown in the dQ/d*V* graph of Figure 5a, which can be used to better understand the effects of the electrolyte additives on the cycling of the cells. In cells free of FEC, a specific reduction peak arises at 0.4 V, just preceding the main tin lithiation event, shown in the inset of Figure 5a. This peak fades in following cycles and can be attributed to the reduction of ethyl-methyl carbonate.[37] This specifies that although EC is a film-formation component in the Gen 2 electrolyte, its reduction is not passivating enough to prohibit the decomposition of EMC. However, when FEC is present, the 0.4 V peak disappears and peaks around 1.7, 0.95, and 0.58 V are apparent. The disappearance of the 0.4 V peak in the presence of FEC suggests that FEC suppresses the decomposition of EMC and is involved in the surface film forming processes during initial activation.

The reaction of tin oxides with Li^+ converting to lithium oxide (Li_2O) and tin occur above 0.4 V vs Li^+/Li^0, typically attributed between 0.7 and 0.5 V,[38−40] an area convoluted with SEI formation. In FEC-containing electrolytes, this region exhibits reduction (negative dQ/d*V*), but no clear peaks throughout cycling. In the absence of FEC, features are observed in this region, particularly between 0.6 and 0.5 V, throughout 40 cycles. Below 0.4 V, typical plateaus for the lithiation into Sn are observed for all the cells, but the lithiation/delithiation peaks are sharper with FEC present

DOI: 10.1021/am508593s
ACS Appl. Mater. Interfaces 2015, 7, 6557−6566

particularly for extended cycling (Figure 5c,d). The nearly identical dQ/dV plots shown in Figure 5b, when the materials cycle with relative high capacity in cycle 5, suggest the material being cycled on both electrodes is highly similar in mass and composition. Figure 5c shows the cycle where the performance of the Gen 2 cell precipitously declines; the peaks related to the reaction of Sn with Li^+ were almost diminished without FEC, whereas they still exist with FEC addition. Hence, a small increase of the specific discharge capacity can be obtained in electrolytes with FEC. Furthermore, the Cu_6Sn_5 phase exists on the porous Sn/Cu foam electrode, and it can be transformed into an intermediate phase of Li_2CuSn and an even higher lithiated phase $Li_{4.4}Sn$ below 0.4 V.[41] Therefore, electrode potential plateaus at 0.38, 0.2, and 0.1 V in the discharge profile reflect both Cu_6Sn_5 and Sn participating in Li alloying, which is consistent with the literature.[7,27]

3.3. Benefits of FEC as a Function of Cycling Rate. It is known that FEC addition is of special importance for the specific operations where charging at fast rate or at low temperature is required as these conditions inevitably result in lithium plating.[14] Figure 6 compares the rate performance of Sn/Cu anodes with different FEC amounts. The batteries are discharged/charged at two rates: 0.06 mA/cm^2 (C/9) and 0.27 mA/cm^2 (C/2). Figure 6 shows that capacity retention is enhanced at high rates for all of the FEC-containing cells. For example, with 2% FEC addition, the relative capacity after 50 cycles at each rate tested maintains 76% (0.03 mA/cm^2), 88% (0.06 mA/cm^2), and 89% (0.27 mA/cm^2), respectively. One proposed reason for this improvement is that FEC molecules can slowly release HF that, in turn, serves as the additive for lithium metal deposition during cycling.[14,42,43] It has also been proposed that electrical properties of SEI films are affected by FEC, e.g., lower interfacial resistance is revealed by electrochemical impedance spectroscopy (EIS).[19,33] As a result, the Li-ion migration through the SEI layer accelerates and electrochemical reaction rate increases.

Figure 6a shows there are minimal differences in charge capacity between cells with different concentrations of FEC, meaning capacity fade rate is not strongly affected by the amount of FEC at moderate cycling rate. At faster rates (C/2, Figure 6b), the FEC-free cell retained capacity longer relative to that found at slower rates, likely due to the short total testing time. The cell containing 5% FEC delivers superior performance compared with the cells containing 2% and 10% FEC including the baseline electrolyte. However, more tests would need to be done to find the optimal FEC concentration at this rate. Recent cycling studies engaging a Sn−Fe−P anode similarly show an increase in cycle life with the addition of FEC, with 10% FEC slightly outperforming a 5% addition.[34] The enhancement is correlated to an increased inorganic and decreased organic nature of the SEI as evaluated by X-ray photoelectron spectroscopy.[34] Overall, our coin cells results highlight the importance of selecting the appropriate concentration of electrolyte additive for different cycling rates, yet to understand why this is, we turned to EQCM-D.

3.4. Interfacial Analysis by EQCM-D of Sn Surface with/without FEC Additive. FEC reacts predominantly on the electrodes' surface, and its presence in the solutions contributes to the SEI layer formation,[17,34,44] leading to differences in cycleablility (capacity, reversibility) and rate performance. Thus, the next step in the analysis is the use of EQCM to better understand the impact of FEC additive on electrode surface chemistry. EQCM has been applied in studies of LIB interfaces to monitor the formation of SEI and to probe the lithium-ion intercalation/deintercalation processes.[21,45−47] We performed EQCM measurements on planar, mirror-like Sn electrodes rather than the porous Sn in order to eliminate putative effects arising from the porous electrode.

Figure 7 presents the real-time recording of the EQCM-D measurement including frequency shifts (Δf) and dissipation

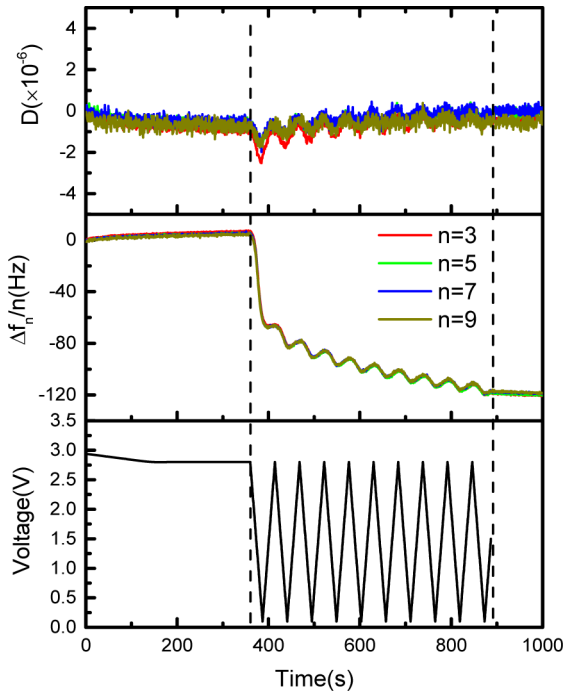

Figure 7. Normalized frequency shifts, $\Delta f_n/n$ and energy dissipation shifts, ΔD_n, vs time obtained for Sn−Cu crystal in Gen 2 at 3rd (n = 3), 5th (n = 5), and 7th (n = 7), and 9th (n = 9) overtones. Drops in frequency correspond with cathodic sweeps (reduction) and rises correspond to anodic sweeps (oxidation) in CV cycling.

changes (ΔD) for various harmonics during CV cycling in Gen 2. Changes in frequency are monitored at this time to assess if significant SEI forms due to spontaneous chemical reactions at OCP, and on these electrodes, it does not. Based on the immediate and rapid frequency change after starting the CV, it appears that the film formation at the electrode−electrolyte interface is fast. The overall decrease in resonant frequency relates to added mass on the Sn surface with cycling time which is associated with a combination of SEI formation, SnO_x conversion, and Cu_6Sn_5/Sn lithiation.

In the traditional QCM analysis using the Sauerbrey relation, mass uptake on the electrode is proportional to the frequency change. However, because there are some cases when the Sauerbrey equation cannot be applied, (for example soft or porous and unevenly deposited film on the electrode surface,)[48] we evaluated the impact of the SEI viscoelastic properties by measuring the energy dissipation of EQCM on the Sn−Cu crystal during SEI formation, SnO_x conversion, and Li insertion/deinsertion, shown in the top panel of Figure 7. The Q-sense EQCM-D system can measure dissipation by turning off the voltage periodically to the sensor, which causes the oscillation to decay. The decay is related to the deposited film properties, like elasticity, viscosity, and structure. A soft film attached to the quartz crystal is deformed during oscillation, which lead to short decay time and gives high

DOI: 10.1021/am508593s
ACS Appl. Mater. Interfaces 2015, 7, 6557−6566

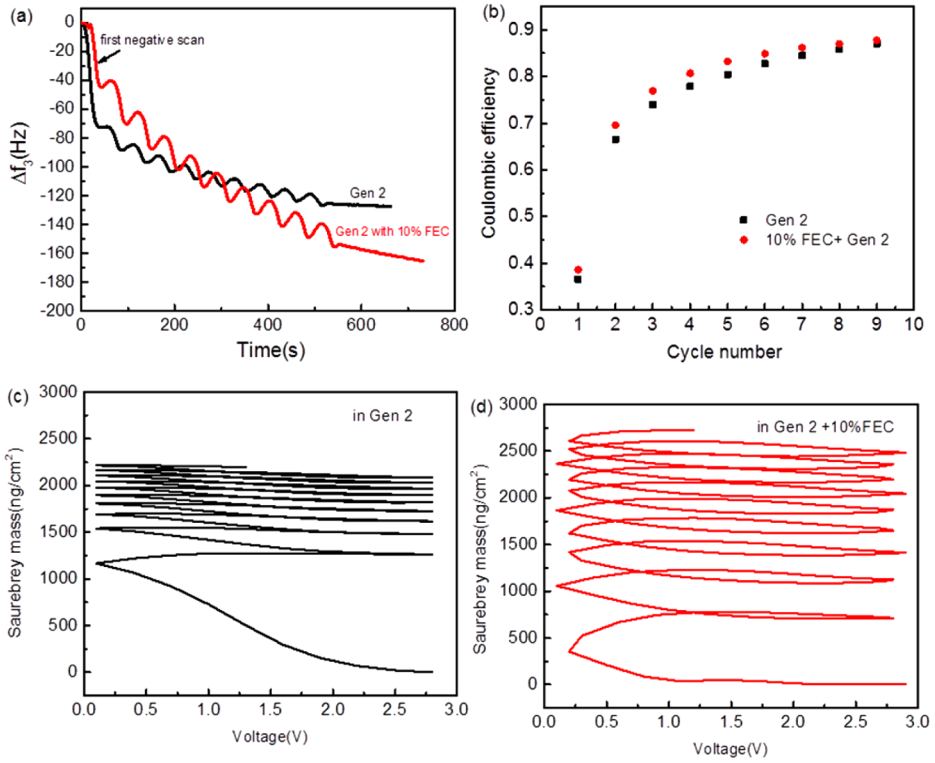

Figure 8. (a) Representative frequency changes in Gen 2 electrolytes with/without 10% FEC. (b) Comparison of Coulombic efficiency for both electrolytes in CV cycling. (c and d) Corresponding mass changes vs potential on Sn surface in Gen 2 electrolytes with/without 10% FEC, respectively. Sauerbrey areal mass was calculated using f_3 overtone, as this overtone signal showed the best signal-to-noise ratio.

dissipation.[25,49] In contrast, for a rigid film the decay time is long and gives a low dissipation. It is noteworthy that D values fluctuate with frequency change during discharge/charge, showing that the structure of deposited film on Sn also changes with cycling. However, the film formation and Li^+ interlation/deinterlation induce relative low total magnitude energy dissipation change as compared to the frequency change. Consequently after 10 cycles of CV scanning, the total frequency change observed from the Gen 2 electrolyte is 120 Hz, while the dissipation remains around zero, as shown in Figure 7. This indicates that the initial SEI forms a rigid structure on the electrode, a result that is equally valid when 10% FEC is added to Gen 2. Moreover, if the frequency data is normalized by overtone number ($\Delta f_3/3$, $\Delta f_5/5$, $\Delta f_7/7$, $\Delta f_9/9$), the identical change in frequency for all overtones will be observed, which suggests the SEI remains mostly rigid and is distributed evenly on the surface during the measurement. Indeed, it is well-known the initial conversion reaction forming a Li_2O layer from SnO_x dominates the response of the electrode both electrochemically and with regard to development of stress. Therefore, the Sauerbrey relation is valid in this system and can be used to estimate the mass.

EQCM-D response upon SEI formation with FEC content in electrolyte was also evaluated under the same CV cycling for an analogous Sn electrode. We used 10 wt % FEC instead of the optimal 2 wt % in order to clarify the effect of FEC addition. Figure 8 compares the frequency change for the 3rd overtone of the cell with and without 10% FEC. The fraction of total anodic to cathodic Coulombs passed per half cycle, described as the Coulombic efficiency of each CV cycle, is shown in Figure 8b. Changes in calculated mass for both cells vs potential are shown in Figure 8c,d. Similar to the one without FEC, there is a steady decrease in frequency response due to continuous film formation on the Sn surface over time. A significant frequency decrease occurs in the first negative scan for both of the cells. Correspondingly, most mass change, ca. 60% of total, occurs during the first reductive wave from OCP to 0.1 V for the cell without FEC. For the cell with FEC, about 30% mass was produced in this potential range. This initial mass gain is associated with the formation of SEI upon electrolyte decomposition, and assuming relatively equal SEI densities, the surface film for the cell without FEC is thicker during the first lithiation process, or there may be a higher efficiency of the conversion reaction in the absence of FEC.

Moreover, the frequency responses coincide with current behavior, that is, the frequency decreases with increasing cathodic current and increases with anodic current, thus representing reversible conversion reactions and Li alloying/dealloying with Sn.[21] However, it should be noted that the frequency increases in the successive positive scans are not completely equal to the absolute value of frequency decreases in negative scans. Therefore, the deposited mass and removed (or decomposed) mass upon every cycle completion are not balanced. The unequal phenomena can be exhibited by the Coulombic efficiency in Figure 8b. The initial Coulombic efficiency is very low due to SEI formation and the conversion reaction. About 80−90% of Li dealloys from Sn during anodic sweeps for the last 5 cycles; however, some Li is left in the Sn after each cycle, i.e., some Li^+ that diffuses into the bulk is not completely delithiated after charging.[47] The Coulombic efficiency is slightly higher in the cell with FEC compared to Gen 2 without FEC, which is consistent with data from galvanostatic cycling in coin cells. It is likely that this "leftover" lithium is related to the observed decrease in cell capacity and

DOI: 10.1021/am508593s
ACS Appl. Mater. Interfaces 2015, 7, 6557−6566

variable rate performance. Alternatively, the larger deposited mass might be partially attributed to continuous SEI growth in the following cycles. The amplitude of frequency variations in each cycle is larger in Gen 2 with FEC than that of the cell without. As the result, after 10 cycles the accumulated mass in Gen 2 with FEC (2770 ng/cm^2) is larger than that of without (2217 ng/cm^2). Roughly 1.3 times more total mass suggests the SEI is continuously growing on the successive cycles in the cell with FEC, which contributes to longer cycle life when we refer back to performance measurements. To summarize, assuming relatively equal SEI densities, the SEI layer without FEC is initially thicker than the SEI layer with FEC. This trend reverses with increased cycling.

Although EQCM measurements do not directly identify the species constituting SEI, we can estimate this information from the mpe (moles per electron) calculation associated with the electrochemical measurements. Figure 9 displays the plot of

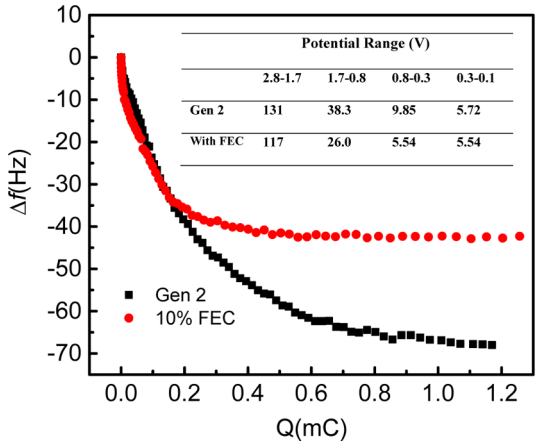

Figure 9. Plot of Δf vs Q for the Sn thin film electrode in the first negative potential scan. The measured mpe values are indicated in the inset table for both systems.

frequency change vs charge change during the first negative sweep in both electrolytes. MPE is calculated from the df/dQ slope and summarized for each system in the Table within Figure 9. It should be noted that mpe does not vary continuously, which suggests that different reduction reactions occur at different voltage stages. When the potential is scanned from OCP (2.8 V) to 1.7 V, the mpe is 131 and 117 g/mol for the cell with and without FEC, respectively. The large initial mpe may be related mainly with the adsorption of solvent molecules on the Sn electrode before their reduction at $E > 1.7$ V. Based on previous spectroscopic studies, the possible decomposition products in EC-containing solutions are $(CH_2OCO_2Li)_2$ (81 g/mol), Li_2CO_3 (37 g/mol), CH_3−OLi (38g/mol), or CH_3OCO_2Li (82 g/mol).[2,45,50,51] The measured mpe (38.3 g/mol) values between 1.7 and 0.8 V in Gen 2 are close to those of CH_3OLi and Li_2CO_3, meaning EC is reduced to CH_3OLi and/or Li_2CO_3 as the major surface reaction. Compared to the mpe value in the cell without FEC, the mpe value is smaller (26.0 g/mol) for the one with 10% FEC in this potential range. This value reflects the formation of LiF (26 g/mol) or LiOH (24 g/mol) is part of the process. Considering the XPS analysis that FEC-derived SEI contains greater concentration of F than EC-based SEI,[15,52,53] we can deduce LiF species are involved in SEI growth with FEC present. It is postulated that increased LiF is due to the preferential reduction of FEC on the electrode surface compared to EC or EMC, thereby suppressing further decomposition of electrolyte. When the potential decreases to 0.8−0.1 V, the mpe should be 7 g/mol if only Li alloying with Sn occurs. The measured value of mpe (9.85 g/mol) between 0.8 and 0.3 V in Gen 2 is close to the theoretical value, indicating in this range the major process consists of Li^+ alloying with Sn. The product of the conversion reaction, Li_2O, has an mpe of 15. The higher mpe in Gen 2 in this range compared to Gen 2 + FEC suggests the conversion reaction may play a larger role on the electrode in the absence of fluorinated EC. However, the lower mpe measured with the addition of FEC might be associated with uncompleted alloying reaction below 0.8 V due to slow kinetics (and fast scan rate). Future studies will focus on the clarification of SEI species produced upon different rates.

4. CONCLUSIONS

In this work, we have investigated the electrochemical performance of composite Sn−Cu anodes in Li-ion half cells cycled with and without the FEC additive. The electrodes were fabricated by simple electroless tin plating on copper foam current collectors and Cu-coated EQCM crystals. The cycling data shows significant differences in lifetime expectations for the 3-D Cu foam current collectors compared to 2-D Cu foils. Better performance could also be expected from the addition of FEC in the electrolytes by changing the basic properties of the solid electrolyte interphase. The comparative studies of different FEC concentrations allow the appropriate additive concentration to be selected based on the demands of the application. EQCM-D was shown to be capable of detecting mass increase and structural changes upon cycling of Sn on Cu vs Li with various electrolytes. In cyclic voltammetry, the SEI layer on Sn electrodes exhibits a dynamic behavior in the sense that it forms significantly during the first negative scan, and on subsequent scans, continues to evolve differently based on electrolyte constituents. Overall, increased SEI/surface mass was measured for the cells containing 10% FEC compared to electrolytes with no additive when formed on Cu−Sn anodes in CV vs lithium.

AUTHOR INFORMATION

Corresponding Author

*L. Trahey. E-mail: trahey@anl.gov.

Notes

The authors declare no competing financial interest.

ACKNOWLEDGMENTS

This work was supported by the Center for Electrochemical Energy Science, an Energy Frontier Research Center funded by U.S. Department of Energy, Office of Science, Office of Basic Energy Sciences.

REFERENCES

(1) Huggins, R. A. Lithium Alloy Negative Electrodes. *J. Power Sources* **1999**, *81*−*82*, 13−19.

(2) Ehinon, K. K. D.; Naille, S.; Dedryvère, R.; Lippens, P. E.; Jumas, J. C.; Gonbeau, D. Ni_3Sn_4 Electrodes for Li-Ion Batteries: Li-Sn Alloying Process and Electrode/Electrolyte Interface Phenomena. *Chem. Mater.* **2008**, *20*, 5388−5398.

(3) Idota, Y.; Kubota, T.; Matsufuji, A.; Maekawa, Y.; Miyasaka, T. Tin-based Amorphous Oxide: A High-Capacity Lithium-Ion-Storage Material. *Science* **1997**, *276*, 1395−1397.

DOI: 10.1021/am508593s
ACS Appl. Mater. Interfaces 2015, 7, 6557−6566

(4) Winter, M.; Besenhard, J. O. Electrochemical Lithiation of Tin and Tin-based Intermetallics and Composites. *Electrochim. Acta* **1999**, *45*, 31−50.
(5) Ortiz, G. F.; Lavela, P.; Knauth, P.; Djenizian, T.; Alcántara, R.; Tirado, J. L. Tin-based composite Materials Fabricated by Anodic Oxidation for the Negative Electrode of Li-Ion Batteries. *J. Electrochem. Soc.* **2011**, *158*, A1094−A1099.
(6) Trahey, L.; Vaughey, J. T.; Kung, H. H.; Thackeray, M. M. High-Capacity, Microporous Cu_6Sn_5-Sn Anodes for Li-Ion Batteries. *J. Electrochem. Soc.* **2009**, *156*, A385−A389.
(7) Nam, D. H.; Kim, R. H.; Han, D. W.; Kwon, H. S. Electrochemical Performances of Sn Anode Electrodeposited on Porous Cu Foam for Li-ion Batteries. *Electrochim. Acta* **2012**, *66*, 126−132.
(8) Mosby, J. M.; Prieto, A. L. Direct Electrodeposition of Cu_2Sb for Lithium-Ion Battery Anodes. *J. Am. Chem. Soc.* **2008**, *130*, 10656−10661.
(9) Park, M.-H.; Kim, M. G.; Joo, J.; Kim, K.; Kim, J.; Ahn, S.; Cui, Y.; Cho, J. Silicon Nanotube Battery Anodes. *Nano Lett.* **2009**, *9*, 3844−3847.
(10) Thackeray, M. M.; Vaughey, J. T.; Johnson, C. S.; Kropf, A. J.; Benedek, R.; Fransson, L. M. L.; Edstrom, K. Structural Considerations of Intermetallic Electrodes for Lithium Batteries. *J. Power Sources* **2003**, *113*, 124−130.
(11) Mao, O.; Dunlap, R. A.; Dahn, J. R. Mechanically Alloyed Sn-Fe(-C) Powders as Anode Materials for Li-Ion Batteries: I. The Sn_2Fe-C System. *J. Electrochem. Soc.* **1999**, *146*, 405−413.
(12) Shin, H.-C.; Liu, M. Three-Dimensional Porous Copper-Tin Alloy Electrodes for Rechargeable Lithium Batteries. *Adv. Funct. Mater.* **2005**, *15*, 582−586.
(13) Yang, C.; Zhang, D.; Zhao, Y.; Lu, Y.; Wang, L.; Goodenough, J. B. Nickel Foam Supported Sn-Co Alloy Film as Anode for Lithium Ion Batteries. *J. Power Sources* **2011**, *196*, 10673−10678.
(14) Zhang, S. S. A Review on Electrolyte Additives for Lithium-Ion Batteries. *J. Power Sources* **2006**, *162*, 1379−1394.
(15) Nakai, H.; Kubota, T.; Kita, A.; Kawashima, A. Investigation of the Solid Electrolyte Interphase Formed by Fluoroethylene Carbonate on Si Electrodes. *J. Electrochem. Soc.* **2011**, *158*, A798−A801.
(16) McArthur, M. A.; Trussler, S.; Dahn, J. R. In Situ Investigations of SEI Layer Growth on Electrode Materials for Lithium-Ion Batteries Using Spectroscopic Ellipsometry. *J. Electrochem. Soc.* **2012**, *159*, A198−A207.
(17) Choi, N. S.; Yew, K. H.; Lee, K. Y.; Sung, M.; Kim, H.; Kim, S. S. Effect of Fluoroethylene Carbonate Additive on Interfacial Properties of Silicon Thin-Film Electrode. *J. Power Sources* **2006**, *161*, 1254−1259.
(18) Applestone, D.; Manthiram, A. Symmetric Cell Evaluation of The Effects of Electrolyte Additives on Cu_2Sb-Al_2O_3-C Nanocomposite Anodes. *J. Power Sources* **2012**, *217*, 1−5.
(19) Liao, L. X.; Zuo, P. J.; Ma, Y. L.; An, Y. X.; Yin, G. P.; Gao, Y. Z. Effects of Fluoroethylene Carbonate on Low Temperature Performance of Mesocarbon Microbeads Anode. *Electrochim. Acta* **2012**, *74*, 260−266.
(20) Komaba, S.; Ishikawa, T.; Yabuuchi, N.; Murata, W.; Ito, A.; Ohsawa, Y. Fluorinated Ethylene Carbonate as Electrolyte Additive for Rechargeable Na Batteries. *ACS Appl. Mater. Interfaces* **2011**, *3*, 4165−4168.
(21) Kwon, K.; Kong, F. P.; McLarnon, F.; Evans, J. W. Characterization of the SEI on a Carbon Film Electrode by Combined EQCM and Spectroscopic Ellipsometry. *J. Electrochem. Soc.* **2003**, *150*, A229−A233.
(22) Santner, H. J.; Korepp, C.; Winter, M.; Besenhard, J. O.; Möller, K.-C. In-Situ FTIR Investigations on the Reduction of Vinylene Electrolyte Additives Suitable for Use in Lithium-Ion Batteries. *Anal. Bioanal. Chem.* **2004**, *379*, 266−271.
(23) Hirasawa, K. A.; Sato, T.; Asahina, H.; Yamaguchi, S.; Mori, S. In Situ Electrochemical Atomic Force Microscope Study on Graphite Electrodes. *J. Electrochem. Soc.* **1997**, *144*, L81−L84.
(24) Leung, K.; Rempe, S. B.; Foster, M. E.; Ma, Y.; Martinez del la Hoz, J. M.; Sai, N.; Balbuena, P. B. Modeling Electrochemical Decomposition of Fluoroethylene Carbonate on Silicon Anode Surfaces in Lithium Ion Batteries. *J. Electrochem. Soc.* **2014**, *161*, A213−A221.
(25) Yang, Z.; Ingram, B. J.; Trahey, L. Interfacial Studies of Li-Ion Battery Cathodes Using in Situ Electrochemical Quartz Microbalance with Dissipation. *J. Electrochem. Soc.* **2014**, *161*, A1127−A1131.
(26) Hubaud, A. A.; Yang, Z.; Dogan, F.; Trahey, L.; Vaughey, J. T. Interfacial Study of the Role of SiO_2 on Si Anodes Using Electrochemical Quartz Crystal Microbalance. *J. Power Sources* **2015**, *282*, 639−644.
(27) Xue, L.; Fu, Z.; Yao, Y.; Huang, T.; Yu, A. Three-Dimensional Porous Sn-Cu Alloy Anode for Lithium-Ion Batteries. *Electrochim. Acta* **2010**, *55*, 7310−7314.
(28) Kravchyk, K.; Protesescu, L.; Bodnarchuk, M. I.; Krumeich, F.; Yarema, M.; Walter, M.; Guntlin, C.; Kovalenko, M. V. Monodisperse and Inorganically Capped Sn and Sn/SnO_2 Nanocrystals for High-Performance Li-Ion Battery Anodes. *J. Am. Chem. Soc.* **2013**, *135*, 4199−4202.
(29) Park, M.-S.; Wang, G.-X.; Kang, Y.-M.; Wexler, D.; Dou, S.-X.; Liu, H.-K. Preparation and Electrochemical Properties of SnO_2 Nanowires for Application in Lithium-Ion Batteries. *Angew. Chem., Int. Ed.* **2007**, *46*, 750−753.
(30) Chen, J.; Yano, K. Highly Monodispersed Tin Oxide/Mesoporous Starbust Carbon Composite as High-Performance Li-Ion Battery Anode. *ACS Appl. Mater. Interfaces* **2013**, *5*, 7682−7687.
(31) Trahey, L.; Kung, H. H.; Thackeray, M. M.; Vaughey, J. T. Effect of Electrode Dimensionality and Morphology on the Performance of Cu_2Sb Thin Film Electrodes for Lithium-Ion Batteries. *Eur. J. Inorg. Chem.* **2011**, *2011*, 3984−3988.
(32) Profatilova, I. A.; Stock, C.; Schmitz, A.; Passerini, S.; Winter, M. Enhanced Thermal Stability of a Lithiated Nano-Silicon Electrode by Fluoroethylene Carbonate and Vinylene Carbonate. *J. Power Sources* **2013**, *222*, 140−149.
(33) Etacheri, V.; Haik, O.; Goffer, Y.; Roberts, G. A.; Stefan, I. C.; Fasching, R.; Aurbach, D. Effect of Fluoroethylene Carbonate (FEC) on the Performance and Surface Chemistry of Si-Nanowire Li-Ion Battery Anodes. *Langmuir* **2011**, *28*, 965−976.
(34) Jang, J. Y.; Park, G.; Lee, S.-M.; Choi, N.-S. Functional Electrolytes Enhancing Electrochemical Performance of Sn-Fe-P Alloy as Anode for Lithium-Ion Batteries. *Electrochem. Commun.* **2013**, *35*, 72−75.
(35) Xia, J.; Sinha, N. N.; Chen, L. P.; Dahn, J. R. A Comparative Study of a Family of Sulfate Electrolyte Additives. *J. Electrochem. Soc.* **2014**, *161*, A264−A274.
(36) Zhang, X.; Kostecki, R.; Richardson, T. J.; Pugh, J. K.; Ross, P. N. Electrochemical and Infrared Studies of the Reduction of Organic Carbonates. *J. Electrochem. Soc.* **2001**, *148*, A1341−A1345.
(37) Smart, M. C.; Ratnakumar, B. V.; Ryan-Mowrey, V. S.; Surampudi, S.; Prakash, G. K. S.; Hu, J.; Cheung, I. Improved Performance of Lithium-Ion Cells with the Use of Fluorinated Carbonate-based Electrolytes. *J. Power Sources* **2003**, *119*, 359−367.
(38) Courtney, I. A.; Dahn, J. R. Electrochemical and in Situ X-ray Diffraction Studies of the Reaction of Lithium with Tin Oxide Composites. *J. Electrochem. Soc.* **1997**, *144*, 2045−2052.
(39) Tavassol, H.; Cason, M. W.; Nuzzo, R. G.; Gewirth, A. A. Influence of Oxides on the Stress Evolution and Reversibility during SnO_x Conversion and Li-Sn Alloying Reactions. *Adv. Energy Mater.* **2014**, *5*.
(40) Courtney, I. A.; Tse, J. S.; Mao, O.; Hafner, J.; Dahn, J. R. Ab Initio Calculation of the Lithium-Tin Voltage Profile. *Phys. Rev. B* **1998**, *58*, 15583−15588.
(41) Fransson, L.; Nordström, E.; Edström, K.; Häggström, L.; Vaughey, J. T.; Thackeray, M. M. Structural Transformations in Lithiated Cu_6Sn_5 Electrodes Probed by in Situ Mössbauer Spectroscopy and X-ray Diffraction. *J. Electrochem. Soc.* **2002**, *149*, A736−A742.
(42) Mogi, R.; Inaba, M.; Iriyama, Y.; Abe, T.; Ogumi, Z. Study of the Decomposition of Propylene Carbonate on Lithium Metal Surface by

DOI: 10.1021/am508593s
ACS Appl. Mater. Interfaces 2015, 7, 6557−6566

Pyrolysis-Gas Chromatography-Mass Spectroscopy. *Langmuir* **2002**, *19*, 814−821.
(43) Chen, L.; Wang, K.; Xie, X.; Xie, J. Effect of Vinylene Carbonate (VC) as Electrolyte Additive on Electrochemical Performance of Si Film Anode for Lithium Ion Batteries. *J. Power Sources* **2007**, *174*, 538−543.
(44) Chen, X.; Li, X.; Mei, D.; Feng, J.; Hu, M. Y.; Hu, J.; Engelhard, M.; Zheng, J.; Xu, W.; Xiao, J.; Liu, J.; Zhang, J.-G. Reduction Mechanism of Fluoroethylene Carbonate for Stable Solid-Electrolyte Interphase Film on Silicon Anode. *ChemSusChem* **2014**, *7*, 549−554.
(45) Aurbach, D.; Moshkovich, M. A study of Lithium Deposition-Dissolution Processes in a Few Selected Electrolyte Solutions by Electrochemical Quartz Crystal Microbalance. *J. Electrochem. Soc.* **1998**, *145*, 2629−2639.
(46) Zhang, X. Y.; Devine, T. M. Identity of Passive Film Formed on Aluminum in Li-Ion Battery Electrolytes with $LiPF_6$. *J. Electrochem. Soc.* **2006**, *153*, B344−B351.
(47) Tavassol, H.; Buthker, J. W.; Ferguson, G. A.; Curtiss, L. A.; Gewirth, A. A. Solvent Oligomerization during SEI Formation on Model Systems for Li-Ion Battery Anodes. *J. Electrochem. Soc.* **2012**, *159*, A730−A738.
(48) Reviakine, I.; Johannsmann, D.; Richter, R. P. Hearing What You Cannot See and Visualizing What You Hear: Interpreting Quartz Crystal Microbalance Data from Solvated Interfaces. *Anal. Chem.* **2011**, *83*, 8838−8848.
(49) Stavila, V.; Volponi, J.; Katzenmeyer, A. M.; Dixon, M. C.; Allendorf, M. D. Kinetics and Mechanism of Metal-Organic Framework Thin Film Growth: Systematic Investigation of HKUST-1 Deposition on QCM Electrodes. *Chem. Sci.* **2012**, *3*, 1531−1540.
(50) Li, J.; Chen, S.-R.; Fan, X.-Y.; Huang, L.; Sun, S.-G. Studies of the Interfacial Properties of an Electroplated Sn Thin Film Electrode/Electrolyte Using in Situ MFTIRS and EQCM. *Langmuir* **2007**, *23*, 13174−13180.
(51) Li, J.; Swiatowska, J.; Maurice, V.; Seyeux, A.; Huang, L.; Sun, S.-G.; Marcus, P. XPS and ToF-SIMS Study of Electrode Processes on Sn-Ni Alloy Anodes for Li-Ion Batteries. *J. Phys. Chem. C* **2011**, *115*, 7012−7018.
(52) Martinez de la Hoz, J. M.; Balbuena, P. B. Reduction Mechanisms of Additives on Si Anodes of Li-Ion Batteries. *Phys. Chem. Chem. Phys.* **2014**, *16*, 17091−17098.
(53) Hong, S.; Choo, M.-H.; Kwon, Y. H.; Kim, J. Y.; Song, S.-W. Interfacial Chemistry Control for Performance Enhancement of Micron Tin-Nickel/Graphite Battery Anode. *J. Electrochem. Soc.* **2014**, *161*, A1851−A1859.

DOI: 10.1021/am508593s
ACS Appl. Mater. Interfaces 2015, 7, 6557−6566